Elasticity of Calcium and Calcium-Sodium Amphiboles

J. Michael Brown* brown@ess.washington.edu
Fax: 206 543 0489

Evan H. Abramson evan@ess.washington.edu

Earth and Space Sciences
University of Washington
Seattle, WA 98195-1310

*Corresponding author

Abstract

Measurements of single-crystal elastic moduli under ambient conditions are reported for nine calcium to calcium-sodium amphiboles that lie in the composition range of common crustal constituents. Velocities of body and surface acoustic waves measured by Impulsive Stimulated Light Scattering (ISLS) were inverted to determine the 13 moduli characterizing these monoclinic samples. Moduli show a consistent pattern: $C_{33}>C_{22}>C_{11}$ and $C_{23}>C_{12}>C_{13}$ and $C_{44}>C_{55}\sim C_{66}$ and for the uniquely monoclinic moduli, $|C_{35}|>>C_{46}\sim|C_{25}|>|C_{15}|\sim 0$. Most of the compositionally-induced variance of moduli is associated with aluminum and iron content. Seven moduli (C_{11} C_{12} C_{13} C_{22} C_{44} C_{55} C_{66}) increase with increasing aluminum while all diagonal moduli decrease with increasing iron. Three moduli (C_{11}, C_{13} and C_{44}) increase with increasing sodium and potassium occupancy in A-sites. The uniquely monoclinic moduli (C_{15} C_{25} and C_{35}) have no significant compositional dependence. Moduli associated with the a^* direction (C_{11} C_{12} C_{13} C_{55} *and* C_{66}) are substantially smaller than values associated with structurally and chemically related clinopyroxenes. Other moduli are more similar for both inosilicates. The isotropically averaged adiabatic bulk modulus does not vary with iron content but increases with aluminum content from 85 GPa for tremolite to 99 GPa for pargasite. Increasing iron reduces while increasing aluminum increases the isotropic shear modulus which ranges from 47 GPa for ferro-actinolite to 64 for pargasite. These results exhibit far greater anisotropy and higher velocities than apparent in earlier work. Compressional velocities are as fast as ~9 km/s and (intermediate between the a^*- and c-axes) are as slow as ~6 km/s. Voigt-Reuss-Hill averaging based on prior single crystal moduli resulted in calculated rock velocities lower than laboratory measurements, leading to adoption of the (higher velocity) Voigt bound. Thus, former uses of the upper Voigt bound can be understood as an *ad hoc* decision to compensate for inaccurate data. Furthermore, because properties of the end-member amphiboles deviate substantially from prior estimates, all predictions of rock velocities as a function of modal mineralogy and elemental partitioning require reconsideration.

Key Words: elasticity, anisotropy, seismic velocities, aggregate elasticity, amphibole, hornblende

1. Introduction

Amphiboles are abundant in crustal igneous and metamorphic rocks. They exhibit a wide range of compositions as a result of extensive solid solution behavior, accommodating all of the abundant cation species (silicon, aluminum, magnesium, iron, calcium, sodium, and potassium). The structure also contains ~2 wt% bound water. When subducted, dehydration reactions in rocks containing amphiboles release water at depth that probably affects the evolution of magma in arc volcanism and is likely associated with intermediate and deep earthquakes (Hacker *et al.* 2003b) as well as seismic tremor/slow slip (Audet et al., 2010).

Since amphiboles are ubiquitous, the description of the crustal seismic structure requires characterization of their elastic properties (*e.g.* Christensen and Mooney 1995, Christensen 1996, Hacker *et al.* 2003a, Barberini *et al.* 2007, Tatham *et al.* 2008, Llana-Funez and Brown 2012, Ji *et al.* 2013, Selway *et al.* 2015). However, knowledge concerning their single-crystal elasticity and compositional dependences has remained elusive. In the pioneering work that continues to be cited, Aleksandrov and Ryzhova (1961a) reported single crystal elastic moduli for two "hornblendes" of unspecified composition based on only slightly over-determined sets of ultrasonic velocity measurements on megacrysts under ambient conditions. As previously demonstrated in studies of feldspars (Brown *et al.* 2006; Brown *et al.* 2016; and Waeselmann *et al.* 2016), results from these early studies have proven to be systematically in error.

That the early ultrasonic results under-estimate velocities most likely was a result of open cleavage surfaces and cracks. Also contributing was an inadequate sampling of velocities as a function of propagation direction. Based on the lack of reported chemistry and probable systematic errors, these early results are considered here in the context of having incorrectly influenced various interpretations of crustal seismic structure that were grounded on mineral properties. In particular, in order to better match laboratory measurements, the compensating use of the upper Voigt bound when calculating aggregate rock velocities has been common. In contrast, Watt and O'Connell (1980) demonstrated that, in well-characterized and nearly crack-free samples, velocities in two phase aggregates fell within the Hashin-Shtrikman bounds which lie between the extremal Voigt and Reuss bounds (see also Watt *et al.* 1976).

A few determinations of single-crystal elastic properties are available within the broad range of amphibole compositions. Bezacier *et al.* (2010) gave elastic moduli for a crystal having a composition near the glaucophane end-member. High pressure x-ray cell parameter determinations have been reported for tremolite, pargasite, and glaucophane (Comodi *et al.* 1991) and for synthetic glaucophane (Jenkins *et al.* 2010).

Hacker *et al.* (2003a) compiled available (isotropically averaged) elasticity data for important rock-forming minerals including amphiboles. They excluded the Aleksandrov and Ryzhova (1961a) moduli as probably being in error and relied on the Christensen (1996) rock velocity measurements to estimate properties of an average crustal "hornblende". To constrain properties of other end-member

compositions, they used Holland and Powell (1998) plus the Comodi *et al.* (1991) compression measurements. Although an isothermal bulk modulus can be inferred from pressure-induced strains, the shear modulus, necessary to estimate body wave velocities, cannot be determined solely from the hydrostatic x-ray data. Instead, Hacker *et al.* (2003a) estimated shear moduli on the basis of the reported bulk moduli and an assumed Poisson's ratio. They noted that this was a remaining source of uncertainty.

As shown later in section 6.3, an isothermal bulk modulus measured under hydrostatic compression (which is equivalent to the elastic aggregate lower-bound Reuss average) is significantly smaller than the appropriate Voigt-Reuss-Hill or Hashin-Shtrikman bulk modulus used for calculation of seismic velocities. Bulk moduli for some amphiboles given by Hacker *et al.* (2003a) appear to represent the Reuss bound. They combined lower bound moduli (in some cases) in an upper-bound Voigt average for calculations of velocities in rocks as mixtures of minerals. Thus, the accuracy of their analysis relied on how well the two errors off-set each other.

Here elastic moduli are reported for nine amphiboles that lie in the range of compositions commonly found in crustal rocks (Schumacher 2007). Elastic wave velocities (body wave and surface wave) were measured using Impulsive Stimulated Light Scattering (ISLS) (Abramson *et al.* 1999). A joint inversion allowed accurate determination of the 13 elastic moduli for these monoclinic minerals. The dependences of moduli on composition are determined through linear regression. From these, relationships to crystal structure and seismic velocities can be explored. Ultimately, more accurate predictions of seismic properties of rocks can be undertaken on the basis of modal mineralogy and elemental partitioning.

2. Amphibole chemistry and structure

As reviewed by Hawthorn and Oberti (2007), the monoclinic (*C2/m*) calcium (including common hornblende) to calcium-sodium amphiboles have a generalized formula of

$$A_{0\text{-}1}B_2C_5T_8O_{22}\,(OH)_2$$

where the A-site is occupied by sodium and potassium or remains vacant and the B-site is occupied by sodium or calcium. The octahedrally coordinated C-sites contain iron (divalent or trivalent), magnesium, or aluminum (designated as ^{vi}Al). The tetrahedral T-sites contain silicon and aluminum (typically up to two aluminum per eight sites, occasionally more, and designated as ^{iv}Al). Other common minor chemical components (Ti, Mn, Co, Cr) are found in size and valence-state appropriate sites. Fluorine and chlorine can substitute for OH^{-1}.

Figure 1

The naming conventions associated with chemistry of calcium and sodium amphiboles (Hawthorne *et al.* 2012, see also Leake *et al.* 1997) are illustrated in Figure 1 using three compositional variables. Aluminum in the T-sites increases from left to right. The site occupancy of A (sodium+potassium) extends in the vertical direction. The solid-solution substitution of sodium for calcium in the B-sites extends into the figure. Although complete solid-solution substitution is

possible within this compositional space, several of the stoichiometric compositions are given discrete names. Tremolite is $[]Ca_2Mg_5Si_8O_{22}(OH)_2$ (where the brackets denote the vacant A-site) while winchite has one calcium and one sodium in the B-site. Glaucophane has all sodium in the B-site with coupled substitutions of a trivalent cation in C-sites required to balance charge. Hornblende is both an end-member in Figure 1 and is a generalized term for calcium amphiboles with intermediate tetrahedral aluminum compositions. In addition, solid-solution substitution of iron for magnesium gives rise to iron end-members for all phases shown in Figure 1 with ferro- added to the name (*e.g.* ferro-pargasite).

Amphiboles have I-beam structures of two double tetrahedral chains that are bonded to each other by an octahedral sheet with five C-site cations. The I-beams are oriented along the *c*-axis with A-site cations (when present) bonding the I-beams along the *a*-axis and B-site cations serving to bond I-beams along the *b*-direction. Clinopyroxenes share similar chemical variations in a structure that is closely related to the amphiboles, both being inosilicates but the pyroxenes have a single tetrahedral chains aligned along the *c*-axis. The general formula of the clinopyroxene is BCT_2O_6 with the B and C sites being equivalent to those found in the amphiboles. End member pyroxenes include diopside ($CaMgSi_2O_6$) hedenbergite ($CaFeSi_2O_6$), and jadeite ($NaAlSi_2O_6$).

Having a wide range of solid-solution substitutions for essentially the same crystal structure, amphiboles provide a natural laboratory for the exploration of chemical controls on elasticity. Variations in elastic moduli are anticipated from changes of ionic sizes and charges, as a result of cation substitutions in the A, B, C and T sites. Comparisons of elasticity between pyroxenes and amphiboles provides further opportunities to explore factors influencing elastic behavior.

3. Sample sources and characterization

The sources, localities (when known), x-ray determined volumes, and densities of nine amphiboles are given in Table 1. Their structural formula, based on Probe-AMPH (Tindle and Webb, 1994), are given in Table 2 and are plotted in perspective in Figure 1. The underlying microprobe measurements are reported in Table S1 of the supporting materials. Samples 1 and 2 with ~1 sodium in the B-site are classified as calcium-sodium amphiboles. The remaining seven samples are calcium amphiboles. The chemistry of the glaucophane sample used by Bezacier *et al.* (2010) and the average calcium amphibole composition reported by Schumacher (2007) are also included in Table 2. As noted by Schumacher (2007), calcium amphiboles cover a wide range of intermediate compositions within the compositional space defined in Figure 1 and his reported average (based on over 1700 published analyses) may be a biased estimator of an average "hornblende" in crustal rocks since samples were analyzed for specific science interests rather than being chosen to best represent crustal chemistry. Nonetheless, this average provides a reference point, defining a common hornblende composition in the following discussion.

Table 1

Table 2

In Figure 2, sample compositions are projected onto pairs of compositional variables. The nine samples used in this study show a range of compositions that generally brackets the averages reported by Schumacher (2007). This is

Figure 2

prerequisite to determining compositional contributions to the elastic properties within the appropriate bounds of elemental partitioning in crustal calcium amphiboles.

The following convention is adopted to align the crystallographic axes with respect to the Cartesian axes for the description of the elastic tensor. The Y axis is aligned parallel to the crystallographic *b*-axis and the Z axis is aligned parallel to the *c*-axis. The X axis is set in the a^*-direction (perpendicular to the *b*- and *c*-axes). Elastic moduli (stiffnesses) are represented by the 6 by 6 matrix C_{ij} using the Voigt convention. The inverse of this matrix is the compliance matrix S_{ij}.

The vertical sum of the first three rows of the compliance matrix gives six strains, β_i, associated with the application of unit hydrostatic stress. Based on 2/m symmetry β_4 and β_6 are zero. These strains can be cast as a 3x3 symmetric tensor which gives crystal compressibility under hydrostatic stress at the limit of zero stress.

4. Experimental methods

Both body wave (compressional and transverse) and surface acoustic wave (SAW) velocities were measured using the method of Impulsive Stimulated Light Scattering (ISLS) (Abramson *et al.* 1999). All measurements (typically between 100 and 200 individual velocity determinations per sample) are reported in Table S2 of the supplementary materials. Details of the experiments and the methods used to determine elastic parameters for low symmetry minerals have been described for body wave measurements (Collins and Brown 1998) and, separately, for SAW measurements (Brown *et al.* 2006).

New in this work is the joint inversion of both body and SAW velocities as described in Brown (2016). Although a complete body wave data set is sufficient to determine all elastic moduli, it proved difficult to obtain a full set of velocities (compressional and two polarizations of transverse waves) for all propagation directions in these natural samples. In some directions, internal flaws scattered light so strongly that the body wave signal could not be recovered from the background and velocities for both polarizations of transverse waves could not be obtained in an adequate number of propagation directions. SAW velocities, based on light coherently scattered from a polished surface, could be more readily measured for all directions of propagation.

The typical *rms* misfit (reported in Table S2) obtained through joint fitting of all measurements is ~0.2%. This is about 12 m/s for SAW and 16-20 m/s for body waves. Such misfits are essentially identical to those previously reported for individually analyzed body wave and SAW mineral data sets (*e.g.* Collins and Brown 1998 and Brown *et al.* 2016) and are representative of intrinsic errors associated with the technique (*e.g.* Abramson *et al.* 1999). Thus, no additional systematic errors appear to have been introduced through joint analysis of body wave and SAW velocity determinations.

The resulting elastic moduli C_{ij} and their associated 2σ uncertainties are listed in Table 3 for the nine amphiboles plus glaucophane. The compliance matrix elements S_{ij} (inverse of the matrix C_{ij}) and compliances sums, β_i, are listed in Table S2. The

sums are also given in principal axis coordinates of the hydrostatic compressibility ellipsoid.

Body wave velocities for glaucophane in Bezacier *et al.* (2010) were reanalyzed using the same numerical optimization methods used here. The velocity misfit was reduced from the previously reported 44 m/s (about 0.5%) to 37 m/s. Some of the new moduli differ by ~2 GPa and some uncertainties given by Bezacier *et al.* (2010) are substantially different from those reported here (see further discussion in Brown 2016). In particular, it would appear that previously reported uncertainties of some off-diagonal moduli were under-estimated and several diagonal uncertainties were over-estimated. Moduli uncertainties for glaucophane are roughly twice as large as those for the calcium and calcium-sodium amphiboles as is appropriate for the observed larger misfit to measured velocities.

5. Elastic moduli and their compositional dependence

Elastic moduli and isotropic body wave velocities are plotted in panels of Figure 3 as a function of total aluminum. Also plotted in the panels are predictions based on fits in chemical composition that are described below. The moduli that are non-zero for orthorhombic crystals are shown in the top three panels. The uniquely monoclinic moduli are plotted in the lower left panel. Adiabatic bulk and shear moduli given as the mean of Hashin-Shtrikman bounds (Brown 2015) are shown in the middle lower panel and the resulting isotropic compressional and transverse wave velocities are in the lower right panel. Figure 3

For all compositions the relative sizes of the moduli remain consistent. That is $C_{33}>C_{22}>C_{11}$ and $C_{23}>C_{12}>C_{13}$, and $C_{44}>C_{55}\sim C_{66}$ and for the uniquely monoclinic moduli, $|C_{35}|>>C_{46}\sim|C_{25}|>|C_{15}|\sim 0$. The same pattern and roughly similar moduli are apparent for glaucophane. However, the C_{22}, C_{33}, and C_{23} moduli of glaucophane are significantly stiffer. As further discussed below, the large value of C_{35} (comparable to the off-diagonal orthorhombic moduli and larger than all other monoclinic moduli) is responsible for a rotation of elastic extrema in the crystallographic plane containing the *a*- and *c*-axes.

Six chemical controls on elasticity associated with changes in cation charges and sizes can be identified as likely to produce significant effects. These are (1) total aluminum content, or its separate content in either (2) T-sites or (3) C-sites, (4) iron content in C-sites (mainly replacing magnesium), the (5) degree of A-site occupation, and (6) sodium replacement of calcium in B-sites. Other possibilities that are less likely to have a measureable impact (including replacement of OH^{-1} with Cl^{-1} or F^{-1}, or changes in the ferric-ferrous iron ratio) could not be studied on the basis of a limited number of samples.

Moduli are assumed to be linear in the six compositional metrics identified above. Tremolite is used as the base composition and changing chemical content is given by the formula unit measures listed in Table 2. A standard statistical measure, the F-test (Rencher 2002), determined the significance of the proposed metrics through stepwise addition and removal of terms using MATLAB® function *stepwiselm.* Only three compositional terms were found to have significant impact at the 95% confidence level; these are total aluminum, A-site occupancy, and iron in the C-site.

Despite the difference in charge and ionic radius, the substitution of sodium for calcium in the B- site appears to have negligible impact on moduli. In addition, at the 95% confidence level, no tested parameterization could reconcile the glaucophane moduli with the calcium and calcium-sodium amphiboles moduli. This suggests that the elasticity of the fully sodium amphibole does not lie on a continuum of linear solid solution behavior or that the experimental uncertainty is larger than estimated. No regression based on compositional "vectors" that are linear combination of the compositional metrics, as suggested by Schumacher (2007), adequately fit the data.

Regression parameters are given in Tables 4 and 5. Blanks in the tables indicate no significant contributions for particular terms. The first column of values gives the estimate for end-member tremolite. Nominal magnesium hornblende (composition as shown in Figure 1) is modeled by adding one aluminum (one times the second column of values for *dM/Al*). For edenite one unit of the third column (*dM/dA*) is added to the hornblende estimate. Fero-actinolite is calculated as the first column (tremolite) plus five times the fourth column (*dM/dFe*), replacing 5 Mg with 5 Fe.

Table 4

Table 5

Average experimental uncertainties for the moduli are in the next to last column and the last column gives the *rms* misfits of the regressions. For the three moduli showing significant sensitivity to A-site occupancy, an alternative model using only total aluminum and iron metrics, is also listed. Most regression misfits are comparable to experimental uncertainty. However, that the regression misfits tend to be larger than experimental uncertainties argue for additional errors or for an incorrectly parameterized chemical dependence. In particular, (1) errors in the determination of sample compositions may be a factor, (2) errors in the moduli may be under estimated, (3) additional compositional metrics may be necessary, or (4) moduli may vary non-linearly with chemistry as was observed in the plagioclase feldspar series (Brown *et al.* 2016).

The regression predictions for moduli and isotropic velocities are shown in Figure 3. Solid lines give the trends associated with increasing aluminum for an iron-free mineral with no A-site occupation. Dashed lines give the predicted behavior of the ferro-equivalent mineral. For moduli showing dependence on A-site occupancy or iron content, the open symbols show predicted moduli. Predicted moduli lie on the solid lines at the appropriate aluminum content if open symbols are not plotted.

All diagonal elastic moduli (and the isotropic average shear modulus) are sensitive to iron; these moduli all decrease with the addition of iron. As seen in Table 4 and in Figure 3, the derivatives of the moduli with respect to iron are similar for all diagonal constants. Seven of thirteen moduli (C_{11} C_{22} C_{13} C_{12} C_{44} C_{55} C_{66}) increase with aluminum content while C_{46} decreases with aluminum. Five moduli (C_{33} C_{23} and the monoclinic moduli C_{15} C_{25} and C_{35}) have no significant dependence on aluminum. Both isotropic moduli (bulk modulus and shear modulus) increase with added aluminum. A small number of moduli (C_{11} C_{13} and C_{44}) are dependent on A-site occupancy. The alternative models with no A-site dependence in Tables 4 and 5 have significantly greater misfit. Note that large deviations between C_{13} values in Figure 3 and the solid line are well predicted by variations in A-site occupation. In Table 5, all three metrics are necessary to adequately predict the variations of

density and the isotropic transverse wave velocities while aluminum and iron content are sufficient to predict compressional velocities.

6. Discussion

6.1 Compositional and structural controls on elasticity

In Table 6 the elastic moduli of several amphibole compositions are compared with chemically related clinopyroxene. Amphibole moduli associated with longitudinal stresses and strains involving the a^*-axis (*ie.* C_{11} C_{12} C_{13} C_{55} C_{66}) are all significantly smaller by approximately a factor of two than the same clinopyroxene moduli while moduli associated with the *b*- and *c*-axes (C_{22} C_{33} C_{23} C_{44}) are notably similar. That (as shown in Table 4) C_{11} and C_{13} increase with increasing A-site occupation seems reasonable since cations in the A-site provide additional bonding and thus additional resistance to compression along the a^*-direction. However, even with full A-site occupations, these amphibole moduli remain smaller than those for pyroxenes (that lack the A-site). The reversal of sign for the uniquely monoclinic moduli (C_{15} C_{25} and most importantly C_{35}) are responsible for a major shift in the orientation of anisotropy between amphiboles and pyroxenes that is further discussed below. With a few exceptions, amphiboles and the compositionally related clinopyroxenes show similar patterns: added aluminum increases some moduli and added iron lowers the diagonal moduli. These trends in amphiboles are further explored through comparison of velocity anisotropy and the hydrostatic-induced strain anisotropy.

Table 6

6.2 Velocity Anisotropy

Compressional and transverse wave velocities are shown in Figure 4 as a function of propagation direction in three orthogonal planes. The orientations of crystallographic axes are shown. Light grey circles indicate velocities of 2, 4, 6, 8 and 9.5 km/s. Dark curves give the velocities for the three elastic waves in each plane. For comparison with the amphiboles, the velocities for a nearly iron-free diopside based on moduli reported by Isaak *et al.* (2006) are shown in the top row; the diopside moduli more recently reported by Sang *et al.* (2011) are in agreement with the Isaak *et al.* results. Below that, velocities for the end member amphibole tremolite based on the current study are shown. Compressional velocities based on the elastic moduli of sample I of Aleksandrov and Ryzhova are also plotted along with tremolite. In the third row velocities for pargasite ($NaCa_2(Mg_4Al)(Si_6Al_2)O_{22}(OH)_2$) based on the current work are shown. The bottom row gives glaucophane velocities based on measurements of Bezacier *et al.* (2010).

Figure 4

Compressional velocities for both diopside and the amphiboles are uniformly most anisotropic in the X-Z plane (containing the *a*- and *c*-axes) and are most isotropic in the Y-Z plane (containing the *b*- and *c*-axes). Although not fully symmetric, compressional velocities in the X-Z plane are roughly ellipsoidal (although diopside maintains higher velocities over a broader range of directions) with the semi-major axis rotated from alignment with the *c*-axis. The diopside semi-major axis is rotated clockwise (associated with positive values for the uniquely monoclinic moduli C_{15} and C_{35}) while the semi-major axis for all amphiboles is rotated counterclockwise (associated with negative values for C_{15} and C_{35}).

The maximum compressional velocity for both the diopside and the iron-free amphiboles is >9 km/s. All amphiboles are more anisotropic than clinopyroxenes as a result of the small values of moduli associated with the a^* direction (C_{11} C_{12} C_{13} C_{55} and C_{66}). The lowest compressional velocity for tremolite is ~6 km/s in a direction ~20° counter-clockwise from the positive a^*. Pargasite (with more aluminum and full occupancy of the A-site) has a larger minimum velocity of ~7 km/s in roughly the same orientation. Glaucophane compressional velocity anisotropy is intermediate between tremolite and pargasite with the semi-major axis located closer to the *c*-axis. Based on the compositional derivatives in Table 4, velocities for iron-rich amphiboles (ie. ferro-actinolite and ferro-pargasite) are substantially lower (8.4 km/s in the fast direction and 5.3 km/s in the slowest direction) as a result of smaller values for the diagonal moduli and larger densities.

The greater transverse wave anisotropy for amphiboles than for clinopyroxene is evident in Figure 4. Amphibole transverse wave anisotropy ranges from a minimum velocity for tremolite of 3.7 km/s and a maximum of 5.2 km/s. Within the *a*-*b* plane transverse velocities for the two transverse wave polarizations are equal in the a^*-direction and show the greatest difference in the *b*-direction.

As shown in Figure 4, velocities based on the hornblende moduli reported by Aleksandrov and Ryzhova (1961a) do not compare well with the current amphibole data. Compressional velocities are both significantly smaller and have less anisotropy as shown in the *b*-*c* plane. The magnitude of the velocity anisotropy and its orientation relative to crystal axes, as illustrated in the *a*-*c* plane, do not match current data. It is likely that these moduli, like the moduli for the feldspars (as previously discussed in Brown *et al.* 2016 and Waesselman *et al.* 2016) are biased as a result of open cleavage surfaces and cracks.

The moduli for amphiboles reported here and the previously reported moduli for plagioclase (Brown *et al.* 2016) and potassium feldspars (Waeselmann *et al.* 2016), taken together, show that all major crustal mineral phases are highly anisotropic. In fact, they are as anisotropic as the sheet silicates phlogopite (Chheda *et al.* 2014) and muscovite (Vaughan and Guggenheim 1986). Thus, any preferred orientations of minerals will lead to rocks that exhibit significantly anisotropic velocities.

In the absence of alternative data, all past efforts to understand crustal seismic anisotropy and the anisotropy measured in rocks with preferred crystal orientations have relied on the moduli reported by Aleksandrov and Ryzhova (1961a, 1961b). A pragmatic choice, compensating for the low moduli has been to use the Voigt average (upper elastic aggregate bound) rather than the more appropriate Hill or Hashin-Shtrikman average (see also the discussion in Brown *et al.* 2016 related to plagioclase minerals). As demonstrated in Figure 4, use of the Aleksandrov and Ryzhova moduli fails to account for the full anisotropy of the amphiboles in rocks containing crystal preferred orientations. It would appear necessary to recalculate properties of amphibole-rich rocks on the basis of more accurate determinations of amphibole elasticity.

394 **6.3 Isotropic moduli and body wave velocities**

395 Estimates for the bulk moduli of calcium and sodium amphiboles are summarized in
396 Table 7. In the top row are the results based on the current work plus glaucophane.
397 The Reuss average adiabatic bulk moduli are corrected to isothermal conditions
398 using thermodynamic properties summarized in Hacker *et al.* (2003a) which results
399 in a reduction by about 1.5%. The values labeled H-S are the mean of the adiabatic
400 Hashin-Shtrikman bounds. Rows labeled C91 (Comodi *et al.* 1991) and J10 (Jenkins
401 *et al.* 2010) give isothermal bulk moduli based on x-ray diffraction studies at high
402 pressure. The second value (plus an uncertainty estimate) for the C91 glaucophane,
403 based on a re-analysis by using EoSFit5.2 (Angel 2001), is smaller by over 8%.
404 Jenkins *et al.* (2010) measured lattice strains in two synthetic glaucophane crystals
405 to 10 GPa and reported an isothermal bulk modulus that lies between the two
406 estimates based on the measurements by Comodi *et al.* (1991) and is larger than the
407 isotropic average of the elastic moduli of Bezacier *et al.* (2010). The last row lists
408 the compilation of bulk moduli (Hacker *et al.* 2003a) used for calculation of
409 compressional and transverse elastic wave velocities in rocks.

410 The range of values given in Table 7 highlight several issues. As apparent in the first
411 row, the large anisotropy of amphiboles leads to large differences between the
412 aggregate bounds. The Reuss-bounded bulk moduli are significantly smaller than
413 the mean of the Hashin-Shtrikman bounds. In addition, the range of glaucophane
414 values based on axes compression measurements indicates that the accuracy of such
415 estimates is highly dependent on the method of analysis and the quality of the data.
416 The compilation of Hacker *et al.* (2003a) has moduli that appear to over-estimate
417 the dependence on iron and to under-estimate the dependence on aluminum. Some
418 of the Hacker *et al.* (2003a) entries are more similar to the Reuss bound while other
419 entries are closer to the mean of the upper and lower aggregate bounds.

420 In Table 8 current estimates for the adiabatic shear modulus are compared with the
421 estimates given by Hacker *et al*. (2003a) that were based on an assumed scaling of
422 Poisson's ratio reported by Christensen (1996). The compilation consistently under-
423 estimates the shear modulus for all amphiboles; this would lead to an under-
424 prediction of transverse wave velocities.

425 Isotropic body wave velocities for amphiboles are shown in Table 9. The values
426 labeled "Literature" are based on Hacker *et al.* (2003a) where two significant figures
427 were given for most elastic moduli. The "hornblende" in that compilation was
428 based on hornblendite velocities reported by Christensen (1996) to four significant
429 figures. Thus, more precision is provided for the hornblende table entries. The
430 values labeled "Current" are based on averages of the Hashin-Shtrikman bounds of
431 moduli as a function of composition. The hornblende entry uses the average
432 calcium amphibole composition given by Schumacher (2007). Several trends are
433 clear for the calcium amphiboles. Increasing aluminum leads to higher
434 compressional velocities but this has less impact on transverse wave velocities.
435 Increasing iron decreases both compressional and transverse wave velocities. The
436 estimates of Hacker *et al*. (2003a) are not consistent with these trends. That the
437 average calcium amphibole has lower density and higher sound speeds than the
438 hornblendite of Christensen (1996) likely reflects a compositional difference

(assuming more aluminum and more iron moves the prediction in the appropriate direction to better match the hornblendite velocities).

Poisson's ratios,

$$\sigma = \frac{1}{2}\left[1 - \left(\left(\frac{V_p}{V_s}\right)^2 - 1\right)^{-1}\right]$$

identified by Christensen (1996) as an important discriminator in the interpretation of crustal seismology, are also listed in Table 9. The near constant values for the "Literature" entries reflect the assumption required in the Hacker *et al.* (2003a) compilation where no independent determination of the shear modulus was available. In the current work, σ is shown to be strongly dependent on the iron content of the amphiboles with low values near 0.21 for tremolite, high values of 0.27 for actinolite, and intermediate value of 0.24 for the calcium amphibole average. Increasing aluminum leads to a small positive increase in σ. The glaucophane of Bezacier *et al.* has the smallest value for Poisson's ratio.

The comparisons made in this section suggest that the predicted isotropic body wave velocities of an average calcium amphibole (hornblende) based on the compositional dependences determined here are in reasonable agreement with laboratory measurements on a hornblendite of unspecified composition. Prior efforts were not able to correctly describe the variation of isotropic elastic wave velocities within the range of amphibole compositions found in crustal rocks.

6.4 Anisotropic strain under hydrostatic stress

Projections on two planes of elastic compressibilities under hydrostatic stress, represented using the compliance sums, β_i, of Table S2 are shown in Figure 5. Three amphiboles (tremolite, pargasite, and glaucophane) and one clinopyroxene (diopside) are plotted. The dashed ellipses are based on the high pressure axis compression analysis of Jenkins *et al.* (2010) while all other ellipses are calculated from elastic moduli measured under ambient conditions. The panel on the left has strains in the crystallographic *a*-*c* plane and the panel on the left has strains in the *b*-*c* plane. Figure 5

All amphiboles have the most compliant direction aligned between *a**- and *c*-axes. The semi-major axis of the natural glaucophane (Bezacier *et al.* 2010) is rotated least from *a** and tremolite is rotated most. Although the synthetic glaucophane axes compressions show near isotropic strain in the *b*-*c* plane, the elastic moduli measurements of a natural crystal show significant anisotropy that is similar to pargasite. Tremolite in the *b*-*c* plane has intermediate anisotropy. The weaker bonding of amphiboles (with vacant or partially filled A- sites) allows greater strain with compression in the general *a*-axis direction. The structurally and compositionally similar mineral diopside is less compliant in this direction. In the *a*-*c* plane, the most and least compressible directions for diopside are rotated by about 90° relative to the amphiboles.

The comparisons made in this section indicate that strain under hydrostatic compression calculated on the basis of elastic moduli measured at ambient pressure

are in general accord with x-ray measurements made at high pressure. However, axes compliances (and the resulting bulk moduli) based on x-ray compression measurements are sensitive to the form of equations of state used to fit the data (*e.g.* multiple entries are given here in Table 7 and in Jenkins *et al.* 2010). Such uncertainty can explain the error in the compositional behavior that was previously associated with amphiboles in the compilation by Hacker *et al.* (2003a) when these measurements provided the only information related to elastic properties of important amphibole end member phases.

7. Summary

The full single-crystal elastic moduli of nine natural calcium to calcium-sodium amphiboles have been measured. In addition, velocities of a previously studied natural sodium amphibole have been re-analyzed within the computational framework used in the current study. Clear trends in the behavior of moduli of the calcium and calcium-sodium amphiboles as a function of composition have been identified. A linear fit based on three chemical measures (total aluminum, total iron, and A-site occupation) accounts for most of the compositionally-induced variance in moduli. A linear fit could not reconcile the sodium amphibole glaucophane with the other amphiboles. Either errors in the data or a non-linear dependence on composition are likely.

The amphiboles and chemically related clinopyroxenes share similar values of moduli except that amphibole moduli related to the a^* direction (C_{11}, C_{12}, C_{13}, C_{55}, *and* C_{66}) are approximately a factor of two smaller. This is likely associated with the partially occupied or vacant A-site which is associated with bonding in the a-axis direction. Increasing occupation of the A-site increases some of these moduli. In contrast, the substitution of sodium for calcium in the B-site has no significant impact on moduli. The substitution of iron in the C-sites decreases all diagonal elastic moduli while leaving off-diagonal moduli unaffected.

The orientation of compressional velocity extrema in the a-c plane is significantly rotated between the amphiboles and the clinopyroxenes. This difference is associated with a large negative value of C_{35} for amphiboles and a large positive value for clinopyroxenes.

The variation of isotropic elastic behavior of amphiboles with composition is important in interpretations of crustal seismology. An earlier compilation (Hacker *et al.* 2003a), could not, on the basis of then extant data, correctly determine such behavior. Parameters are provided here that allow accurate determination of the isotropic bulk and shear moduli of common amphiboles in crustal rocks.

It is noteworthy that amphiboles have higher elastic wave velocities and are more anisotropic than suggested by the early measurements of Aleksandrov and Ryzhova (1961a). In fact, amphiboles exhibit anisotropy nearly as large as that observed in sheet silicates (Aleksandrov and Ryzhova 1961b; Vaughan and Guggenheim 1986; Chheda *et al.* 2014) and the feldspars (Brown *et al.* 2006; Brown *et al.* 2016; and Waeselmann *et al.* 2016).

In efforts to reconcile laboratory measurements on rocks with predictions based on the single-crystal moduli reported by Aleksandrov and Ryzhova (1961a and 1961b), the *ad-hoc* use of the upper-bound Voigt average is common. This provided partial, but inappropriate, compensation for under-estimated moduli. Furthermore, the earlier moduli fail to account for the full anisotropy of amphiboles. Thus, all predictions of the seismic response of rocks with preferred crystal orientations will need to be re-evaluated.

Acknowledgments

Support from the National Science Foundation EAR-0711591 enabled this research. The following students helped prepare samples and collect data: N. Castle, E. Chang, S. Pendleton, K. Pitt, K. Straughan, A. Teel, and H. West-Foyle. The microprobe analyses of S. Kuehner and N. Castle and x-ray analyses of W. Kaminsky were vital contributions to this work. B.W. Evans contributed samples and maintained continuing discussions. The RRUFF database and materials provided by R. Downs are highly appreciated. This research was inspired by a course offered by N. I. Christensen in 1974 on the elasticity of minerals and seismic structure of the crust. It was co-attended by M. Salisbury, D. Fountain, and R. L. Carlson. The science contributions and continued enthusiasm of these colleagues is gratefully acknowledged.

References

Abramson, E. H., Brown, J. M., and Slutsky, L. J. (1999) Applications of impulsive stimulated scattering in the Earth and planetary sciences, Annu. Rev. Phys. Chem., 50, 279–313.

Aleksandrov, K. S., Ryzhova, T. V. (1961a) The elastic properties of rock-forming minerals: pyroxenes and amphiboles, Bulletin. USSR Academy of Science, Geophysics, Ser. 9, 871–875.

Aleksandrov, K. S., Ryzhova, T. V. (1961b) Elastic properties of rock-forming minerals II. Layered silicates, Bulletin. USSR Academy of Science, Geophysics, Ser. 9, 1165-1168.

Angel R. J. (2001) EOS-FIT V5.2 users guide. http://www.crystal.vt.edu/crystal/software.html. Program revision August 2008

Audet P., Bostock M. G., Boyarko D. C., Brudzinski M. R. and Allen R. M. (2010) Slab morphology in the Cascadia fore arc and its relation to episodic tremor and slip. J. Geophys. Res., **115**,

Barberini, V., Burlini, L., Zappone, A. (2007) Elastic properties, fabric and seismic anisotropy of amphibolites and their contribution to the lower crust reflectivity, Tectonophysics, 445, 227–244.

Bezacier, L., Reynard, B., Bass, J. D., Wang, J., Mainprice, D. (2010) Elasticity of glaucophane, seismic velocities and anisotropy of the subducted oceanic crust, Tectonophysics, 494, 201–210.

Brown, J. M. (2015), Determination of Hashin-Shtrikman bounds on the isotropic effective elastic moduli of polycrystals of any symmetry, Comput. Geosci., 80, 95–99, doi:10.1016/j.cageo.2015.03.009.

Brown, J.M., (2016) Determination of elastic moduli from measured acoustic velocities, Comput. Geosci., submitted

Brown, J. M., Angel, R. J., and Ross, N. L. (2016) Elasticity of plagioclase feldspars, J. Geophys. Res. Solid Earth, 121, doi:10.1002/2015JB012736.

Brown, J. M., Abramson, E. H., Ross, R. L. (2006) Triclinic elastic constants for low albite, Phys. Chem. Minerals, 33, 256-265.

Chheda, T. D., Mookherjee, M., Mainprice, D., dos Santos, A. M., Molaison, J. J., Chantel, J., Manthilake, G., Bassett, W. A. (2014), Structure and elasticity of phlogopite under compression: Geophysical implications, Phys. Earth Planet. Int., 233, 1-12, doi:10.1016/j.pepi.2014.05.004

Christensen, N. I., and Mooney, W. D. (1995) Seismic velocity structure and composition of the continental crust: A global view, J. Geophys. Res., 100, 9761–9788.

578 Christensen, N. I. (1996) Poisson's ratio and crustal seismology, J Geophys. Res., 101,
579 3139-3156.

580 Collins, M. C., and Brown, J. M. (1998) Elasticity of an upper mantle clinopyroxene,
581 Phys. Chem. Min., 26, 7-13.

582 Comodi, P., Mellini, M., Ungaretti, L., Zanazzi, P.F. (1991) Compressibility and high
583 pressure structure refinement of tremolite, pargasite and glaucophane, Eur. J.
584 Mineral., 3, 485–499.

585 Hacker, B. R., Abers, G. A. & Peacock, S. M. (2003a). Subduction factory, 1,
586 Theoretical mineralogy, density, seismic wave speeds, and H_2O content. J. Geophys.
587 Res., 108, 2029, doi:10.1029/2001JB001127.

588 Hacker, B. R., Peacock, S. M., Abers, G. A. and Holloway, S. D. (2003b) Subduction
589 factory, 2, Are intermediate-depth earthquakes in subducting slabs linked to
590 metamorphic dehydration reactions?, J. Geophys. Res., 108, 2030,
591 doi:10.1029/2001JB001129.

592 Hawthorn, F.C., Oberti, R. (2007) Amphiboles: Crystal chemistry, Rev. Mineral. &
593 Geochem., 67, 1-54.

594 Hawthorne, F.C., Oberti, R., Harlow, G.E., Maresch, W. V., Martin, R. F., Schumacher, J.
595 C., Welch, M. D. (2012) Nomenclature of the amphibole supergroup, Am. Mineral.,
596 97, 2031–2048.

597 Holland, T. J. B., and Powell, R. (1998) An internally consistent thermodynamic data
598 set for phases of petrological interest, J. Metamorph. Geol., 16, 309–343, 1998.

599 Isaak, D. G., Ohno, I., Lee, P.C. (2006) The elastic constants of monoclinic single-
600 crystal chrome-diopside to 1,300 K, Phys. Chem. Miner., 32, 691–699 DOI
601 10.1007/s00269-005-0047-9.

602 Jenkins, D. M., Corona, J. C., Bassett, W. A., Mibe, K., Wang, Z. (2010) Compressibility
603 of synthetic glaucophane, Phys. Chem. Minerals, 37, 219–226 DOI 10.1007/s00269-
604 009-0326-y.

605 Ji, S., Shao, T., Michibayashi, K., Long, C., Wang, Q., Kondo, Y., Zhao, W., Wang, H., and
606 Salisbury, M.H. (2013) A new calibration of seismic velocities, anisotropy, fabrics,
607 and elastic moduli of amphibole-rich rocks, J. Geophys. Res.: Solid Earth, 118, 4699–
608 4728, doi:10.1002/jgrb.50352, 2013

609 Kandelin, J., Weidner, D. J. (1988a) Elastic properties of hedenbergite, J. Geophys.
610 Res., 93, 1063-1072.

611 Kandelin, J., Weidner, D. J. (1988b) The single crystal properties of jadeite, Phys.
612 Earth Planet. Inter., 50, 251-260.

613 Leake, B.E., Woolley, A.R., Arps, C. E. S. Birch, W. D., Gilbert, M. C., Grice, J. D.,
614 Hawthorne, F. C. Kato, A., Kisch, H. J. Krivovichev, V. G. Linthout, K., Laird, J.

615 Mandarino, J. A., Maresch, W. V., Nickel, E. H., Rock, N. M. S., Schumacher, J. C., Smith,
616 D. C., Stephenson, N. C. N., Ungaretti, L., Whittaker, E. J. W., Youzhi, G., (1997)
617 Nomenclature of amphiboles: Report of the subcommittee on amphiboles of the
618 International Mineralogical Association Commission on New Minerals and Mineral
619 Names, Canadian Mineral., 35, 219-246.

620 Llana-Funez, S., Brown, D. (2012) Contribution of crystallographic preferred
621 orientation to seismic anisotropy across a surface analog of the continental Moho at
622 Cabo Ortegal, Spain, Geol. Soc. Amer. Bul., 124, 1495-1513

623 Rencher, A. C. (2002) Methods of Multivariable Analysis, John Wiley & Sons, New
624 York.

625 Sang, L., Vanpeteghem, C.B., Sinogeikin, S.V., and Bass, J.D. (2011) The elastic
626 properties of diopside, $CaMgSi_2O_6$, Am. Mineral., 96*, 224–227*

627 Schumacher, J.C. (2007) Metamorphic amphiboles: Composition and coexistence,
628 Rev. Min. & Geochem, 67, 359-416.

629 Selway, K., Ford, H., Kelemen, P. (2015) The seismic mid-lithosphere discontinuity,
630 Earth Planet. Sci. Lett., 414, 45-57.

631 Seront, B., Mainprice, D., and Christensen, N. I. (1993), A determination of the 3-
632 dimensional seismic properties of anorthosite—Comparison between values
633 calculated from the petrofabric and direct laboratory measurements, J. Geophys.
634 Res., 98, 2209–2221, doi:10.1029/92JB01743.

635 Tatham, D. J., Lloyd, G. E., Butler, R. W. H., Casey, M. (2008) Amphibole and lower
636 crustal seismic properties, Earth Planet. Sci. Lett., 267, 118–128

637 Tindle, A.G., Webb, P.C. (1994) Probe-AMPH—A spreadsheet program to classify
638 microprobe-derived amphibole analyses, Comput. & Geosci., 20, 1201-1228.

639 Vaughan, M.T., Guggenheim, S. (1986) Elasticity of muscovite and its relationship to
640 crystal structure. J. Geophys. Res. 91, 4657–4664.

641 Waeselmann, N, Brown, J. M., Angel, R, J., Ross, N., Zhao, J., and Kaminsky, W. (2016)
642 The elastic tensor of monoclinic alkali feldspars, Am. Mineral., doi:10.2138/am-
643 2015-5583.

644 Watt, J. P., Davies, G. F. and O'Connell, R. J. (1976) The elastic properties of
645 composite materials, Rev. Geophys. Space Phys., 14, 541-563.

646 Watt, J. P. and O'Connell, R. J. (1980) An experimental investigation of the Hashin-
647 Shtrikman bounds on two-phase aggregate elastic properties, Phys Earth Planet Int.,
648 21, 359-370.

Figures

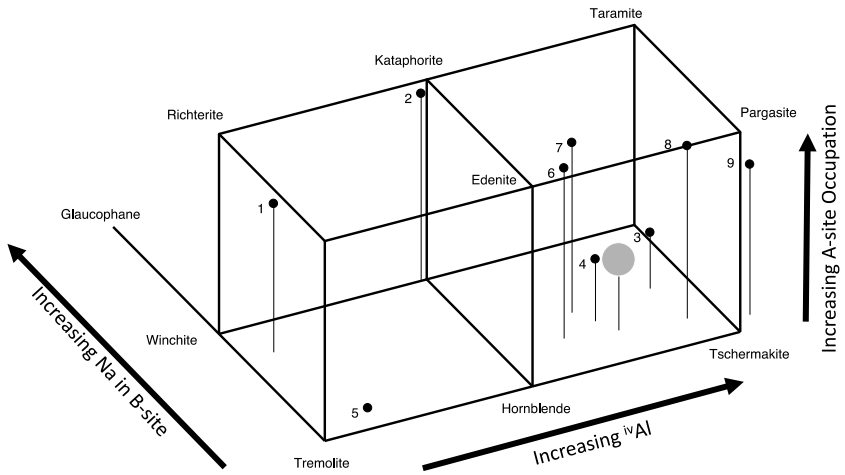

Figure 1. Classification and compositions of magnesium calcium amphiboles plus glaucophane (based on Leake et al. 1997). The axis extending to the right gives increasing aluminum in tetrahedral coordination (from 0 for tremolite to $(Al_2Si_6O_{22})$ for tschermakite). Occupancy of the A-site by (Na+K) (from 0 to 1) is shown in the vertical direction. Substitution of Na for Ca in the B-site extends into the figure with full replacement of Ca by Na found in glaucophane. Named stoichiometric end-member compositions are identified. Full solid-solution replacement of magnesium by iron is labeled by adding ferro- to the end-member names (exceptions ferro-actinolite is the iron-bearing form of tremolite). Small filled and numbered circles are compositions of the current samples based on the chemistry provided in Table 2. The large gray circle gives the average chemistry for calcium amphiboles reported by Schumacher (2007). Lines projected to the zero of A-site occupation are provided as an aid in visualizing the sample compositions.

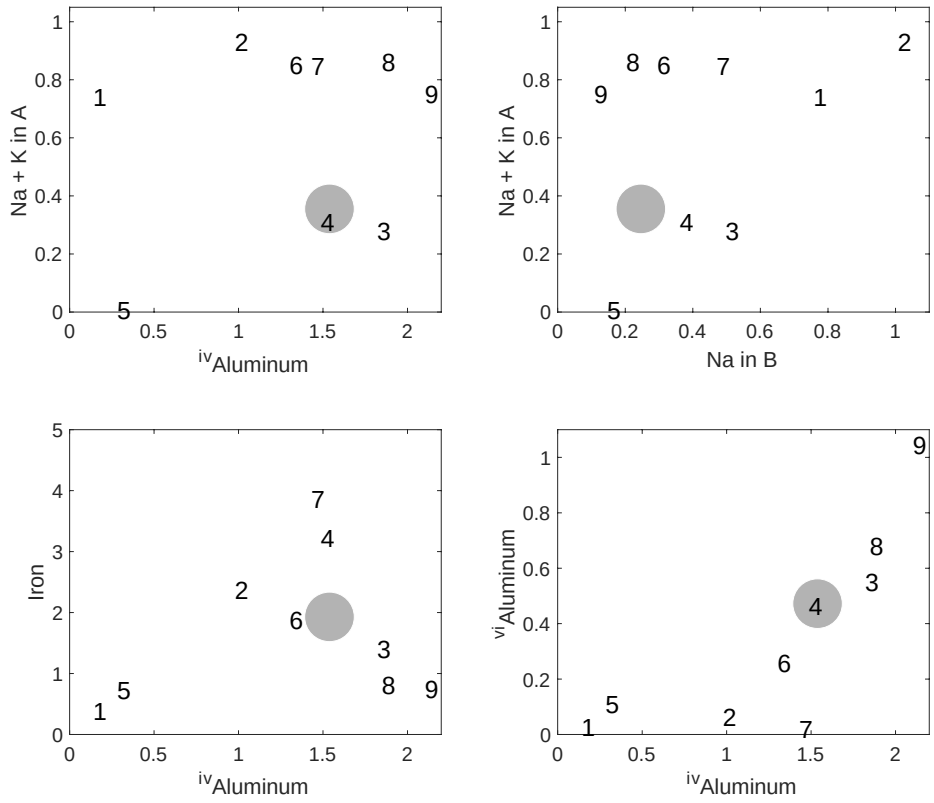

664

665 Figure 2. Compositions of the amphibole samples in formula units reported in Table
666 2. Plotted numbers correspond to the sample numbers. The gray circle is the
667 average of calcium amphiboles reported by Schumacher (2007). The top two panels
668 show front and side projections of the compositions illustrated in Figure 1
669 (tetrahedral coordinated aluminum versus A-site occupation and sodium in the B-
670 site vs A-site occupation). The lower left panel shows the number of iron atoms per
671 formula unit vs tetrahedral coordinated aluminum. The lower panel on the right
672 shows octahedral-coordinated aluminum versus tetrahedral-coordinated aluminum.

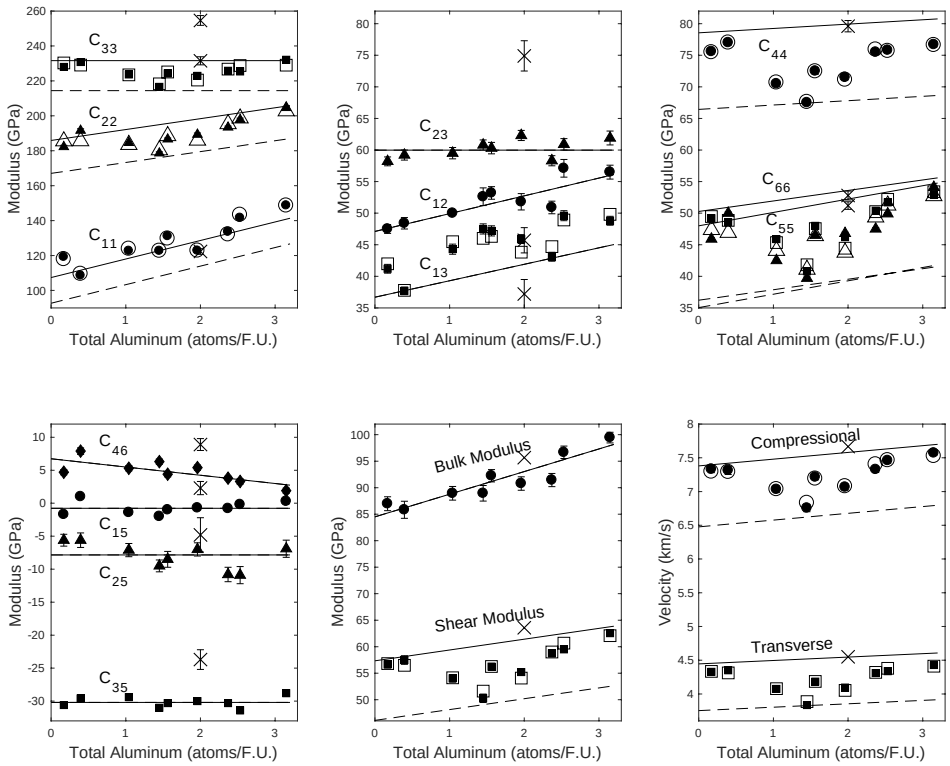

673

674 Figure 3. Elastic moduli and velocities of amphiboles as a function of total aluminum.
675 Filled symbols are current experimental results with error bars shown when larger
676 than the plotted symbol. The different symbol shapes are associated with particular
677 moduli as labeled in each panel. Points with the X symbols are moduli and velocities
678 for glaucophane (Bezacier *et al.* 2010). Solid lines are regression predictions for
679 increasing aluminum content in an iron-free mineral. Dashed lines (when present)
680 give the predicted ferro-equivalent behavior. Open symbols (when present) give the
681 prediction of moduli sensitive to iron or A-site occupancy. When no open symbol is
682 plotted, the predicted moduli lie on the solid lines at the appropriate aluminum
683 content.

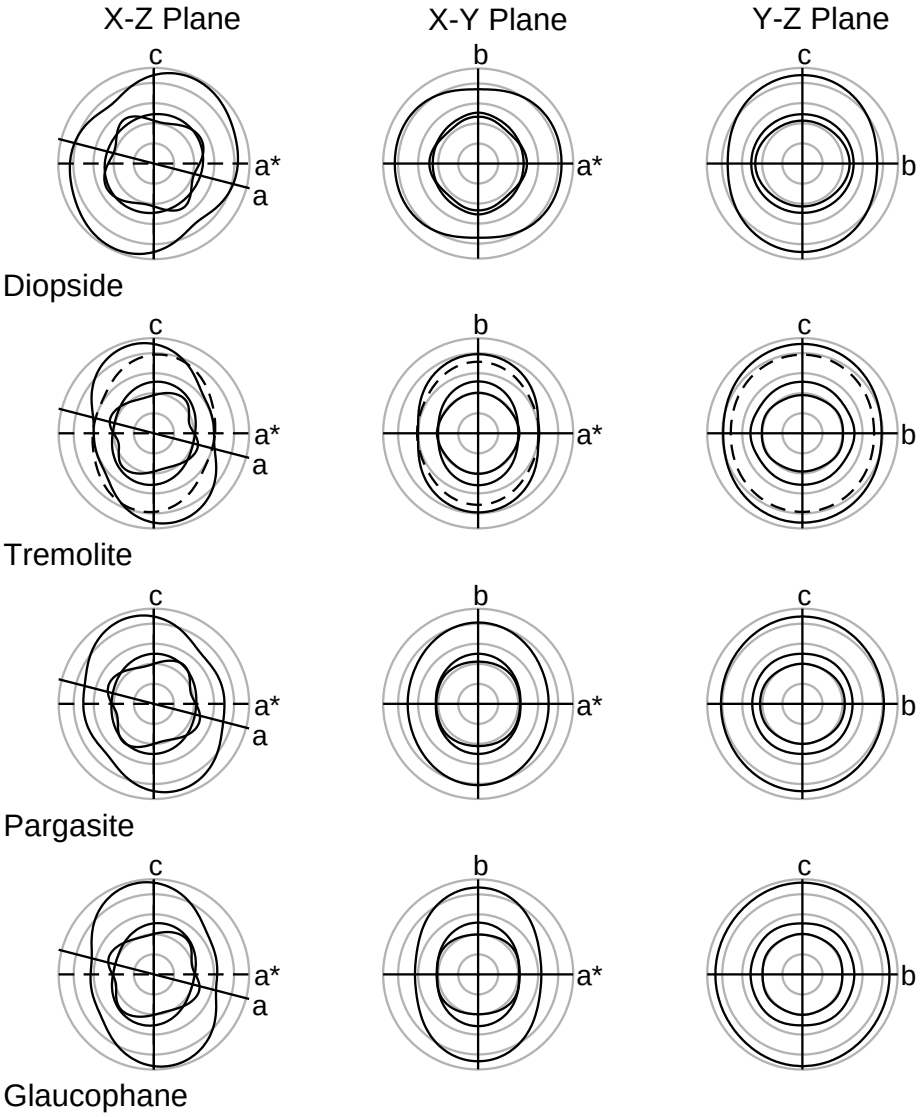

684

685 Figure 4. Selected inosilicate elastic wave velocities as a function of propagation
686 direction in three orthogonal planes. For each plane normal to a Cartesian axis light
687 circles represent velocities of 2, 4, 6, 8, and 9.5 km/s. The orientations of
688 crystallographic axes are shown. Thick line are velocities based on the elastic
689 moduli and propagation directions. The inner thick lines are transverse wave
690 velocities, the outer thick line gives compressional velocities. Top row: diopside
691 velocities based on Isaak *et al.* (2006). Second and third rows: calcium amphibole
692 end-member velocities based on the current work. Dashed line in second row are
693 compressional velocity predictions based on the elastic moduli for a hornblende
694 reported by Aleksandrov and Ryzhova (1961a). Bottom row: glaucophane velocities
695 based on Bezacier *et al.* (2010).

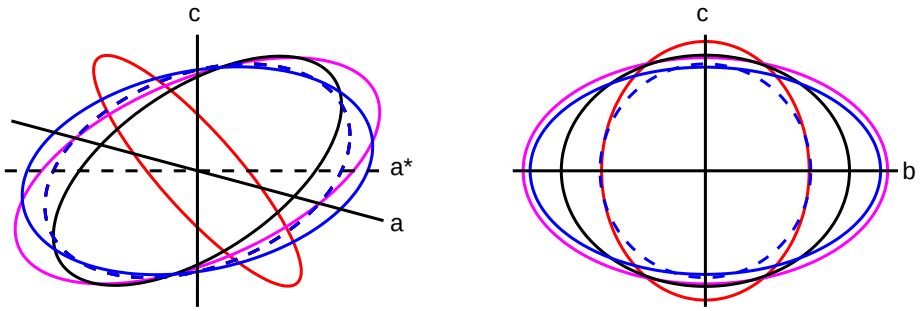

696

697 Figure 5. Selected inosilicate strain ellipsoids under hydrostatic stress projected on
698 the crystallographic *a*-*c* and *b*-*c* planes. Red: diopside from Isaak *et al.* (2006), Black:
699 tremolite from current work, Magenta: pargasite from current work), Blue:
700 glaucophane. Solid line is based on Bezacier *et al.* (2010) and dashed is from Jenkins
701 *et al.* (2010).

Tables

Sample	Unit cell volume ($A^{\circ 3}$)	Density kg/m^3	Source
1	905.7	3027	unknown
2	914.3	3255	unknown
3	901.9	3162	Gore Mountain NY, collected by B.W. Evans
4	913.6	3293	unknown
5	908.4	3038	Lake Wenatchee, WA collected by B.W. Evans
6	918.1	3213	RRuff.info #60029 R. Downs
7	934.0	3418	RRuff.info #60044 R. Downs
8	907.2	3163	RRuff.info #60632 R. Downs
9	895.2	3190	Unknown

Table 1. Amphibole sample information. "Unknown" samples were obtained as mineral separates from rocks of unknown origin. Unit cell volumes are from x ray analysis, densities are calculated based on unit cell volumes and microprobe determined chemistry. The uncertainty in unit cell volume is 0.3%. The density uncertainty, accounting for chemistry and volume uncertainties, is 0.5%.

Sample	1	2	3	4	5	6	7	8	9	GL	HBL
Structural Formulae											
Si	7.859	7.023	6.182	6.513	7.718	6.698	6.571	6.152	5.898	7.76	6.458
Al^{iv}	0.141	0.977	1.818	1.487	0.282	1.302	1.429	1.848	2.102	0.24	1.542
Al^{vi}	0.032	0.064	0.553	0.464	0.113	0.259	0.015	0.683	1.047	1.76	0.470
Ti	0.013	0.109	0.112	0.173	0.002	0.060	0.239	0.319	0.021	-	0.123
Cr	0.000	0.002	0.001	0.000	0.035	0.000	0.000	0.002	0.211	-	0.001
Fe^{3+}	0.097	0.769	1.263	0.727	0.494	0.365	0.559	0.000	0.157	-	0.718
Fe^{2+}	0.287	1.601	0.150	2.004	0.244	1.526	3.298	0.815	0.592	0.92	1.201
Mn	0.028	0.157	0.012	0.030	0.040	0.049	0.205	0.007	0.013	-	0.034
Mg	4.543	2.298	2.910	1.601	4.072	2.741	0.684	3.105	2.958	2.34	2.453
Ca	1.243	0.993	1.503	1.639	1.741	1.706	1.528	1.798	1.892	0.06	1.752
Na	1.236	1.674	0.683	0.577	0.146	0.805	0.981	0.696	0.789	1.90	0.480
K	0.264	0.265	0.088	0.095	0.009	0.341	0.339	0.370	0.071	-	0.121
F	0.937	0.695	0.000	0.000	0.035	0.732	0.000	0.263	0.005	-	0.000
Cl	0.002	0.015	0.000	0.008	0.000	0.030	0.000	0.005	0.000	-	0.000
OH*	1.060	1.290	2.000	1.992	1.965	1.238	2.000	1.732	1.995	2	2.000
Total	17.743	17.932	17.275	17.310	16.895	17.852	17.848	17.795	17.752	-	17.353
Site Occupancy											
(Ca+Na) (B)	2.000	2.000	2.000	2.000	1.887	2.000	2.000	2.000	2.000	1.96	2.000
Na (B)	0.757	1.007	0.497	0.361	0.146	0.294	0.472	0.202	0.108	1.90	0.248
(Na+K) (A)	0.743	0.932	0.275	0.310	0.009	0.852	0.848	0.864	0.752	-	0.353
$Mg/(Mg+Fe^{2})$	0.941	0.589	0.951	0.444	0.943	0.642	0.172	0.792	0.833	-	0.671
$Fe^{3}/(Fe^{3}+Al^{vi})$	0.750	0.923	0.696	0.610	0.814	0.585	0.974	0.000	0.130	-	0.604

Table 2. Microprobe chemical analysis in formula units based on Probe-AMPH (Tindle and Webb, 1994) plus the chemical analysis of the glaucophane (GL) sample used in Bezacier et al. (2010) and the average calcium amphibole (HBL) as reported by Schumacher (2007). See supplemental table for weight % oxides measured by microprobe analysis.

	1	2σ	2	2σ	3	2σ	4	2σ	5	2σ	6	2σ	7	2σ	8	2σ	9	2σ	Gl	2σ
C_{11}	119.2	0.8	122.7	0.9	133.6	0.9	122.8	0.9	108.6	0.7	131.1	0.9	122.7	0.9	141.6	0.9	148.7	1.0	121.5	1.6
C_{12}	47.5	0.7	50.0	0.3	50.9	1.0	51.8	1.3	48.4	0.9	53.2	1.0	52.6	1.4	57.1	1.4	56.5	1.1	44.4	2.0
C_{13}	41.2	0.7	44.3	0.8	43.1	0.7	45.9	0.7	37.7	0.6	47.2	0.8	47.5	0.8	49.6	0.8	48.8	0.7	37.4	2.3
C_{15}	-1.7	0.3	-1.4	0.3	-0.8	0.3	-0.7	0.3	1.0	0.3	-1.0	0.3	-2.0	0.3	-0.2	0.3	0.3	0.4	2.7	1.0
C_{22}	182.2	1.3	184.6	1.2	193.4	1.2	189.3	1.3	191.6	1.4	186.6	1.2	178.6	1.2	197.8	1.3	204.6	1.3	229.7	2.3
C_{23}	58.2	0.8	59.5	0.9	58.3	0.9	62.3	0.9	59.2	0.9	60.3	0.9	60.8	0.9	60.9	1.0	61.9	1.1	75.8	2.4
C_{25}	-5.6	0.9	-7.1	1	-10.8	1.1	-7.0	1.0	-5.6	1.1	-8.5	1.2	-9.5	0.9	-10.9	1.3	-6.9	1.3	-4.9	2.6
C_{33}	228.0	1.5	223.7	1.5	225.8	1.4	222.9	1.4	230.8	1.5	224.3	1.4	216.6	1.3	225.4	1.6	232.1	1.5	256.2	2.8
C_{35}	-30.6	0.5	-29.4	0.5	-30.3	0.4	-30.0	0.4	-29.6	0.5	-30.3	0.5	-31.0	0.4	-31.4	0.5	-28.8	0.5	-23.9	1.5
C_{44}	75.6	0.6	70.5	0.5	75.5	0.6	71.5	0.5	77.0	0.6	72.5	0.6	67.5	0.5	75.8	0.6	76.7	0.6	79.3	0.9
C_{46}	4.7	0.4	5.3	0.4	3.8	0.3	5.4	0.4	7.9	0.5	4.4	0.4	6.3	0.4	3.3	0.4	1.9	0.4	9.3	0.9
C_{55}	45.9	0.3	42.5	0.3	47.5	0.3	46.8	0.3	50.0	0.3	46.5	0.3	39.7	0.3	49.9	0.3	54.1	0.3	52.9	0.7
C_{66}	49.2	0.4	45.9	0.3	50.4	0.3	46.2	0.4	48.6	0.4	48.0	0.4	40.8	0.3	51.7	0.4	52.9	0.4	51.3	0.6

Table 3. Elastic moduli (in GPa) of amphiboles. The 2σ uncertainties include misfits to velocities and uncertainty in sample densities. The column labeled "Gl" gives re-analyzed moduli and uncertainties for glaucophane based on velocities reported by Bezacier et al (2010).

	Modulus GPa	*dM/dAl* GPa/atom	*dM/dA* GPa/atom	*dM/dFe* GPa/atom	Experimental Uncertainty GPa	Regression Misfit GPa
C_{11}	107.2	10.6	13.3	-2.9	1.0	1.1
	109.1	11.4			1.0	5.0
C_{12}	47.1	2.8			1.2	1.6
C_{13}	36.7	2.6	6.5		0.8	1.2
	39.6	3.1			0.8	2.4
C_{15}	-0.8				0.3	0.9
C_{22}	185.9	6.2		-3.8	1.2	2.7
C_{23}	60.0				1.0	1.4
C_{25}	-7.8				1.2	1.9
C_{33}	231.6			-3.4	1.5	2.1
C_{35}	-30.2				0.5	0.8
C_{44}	78.5	0.7	-3.0	-2.4	0.6	0.2
	78.0			-2.5	0.6	1.1
C_{46}	6.7	-1.3			0.4	1.1
C_{55}	48.0	2.1		-2.6	0.4	1.9
C_{66}	50.3	1.7		-2.8	0.4	0.8
K	84.5	4.3			1.2	1.7
G	57.5	2.0		-2.2	0.8	0.8

717

718 Table 4. Linear regression parameters for amphibole individual elastic moduli and
719 the mean of Hashin-Shtrikman bounds for the adiabatic bulk (K) and shear (G)
720 modulus. Base moduli for tremolite are in the first column of values. Derivatives are
721 in units of modulus change per substitutional atom in the formula unit relative to
722 tremolite; the aluminum content varies from 0 to >3, the A-site occupation ranges
723 from 0 to 1, and iron in the C-site can range from 0 to 5. Only C_{11}, C_{13} , and C_{44} have a
724 statistically significant dependence on the A-site occupation. An alternative fit with
725 no dependence on A-site occupation is provided (with a concomitant increase in
726 misfit). The last two columns give experimental and regression misfits.

727

	M	*dM/dAl*	*dM/dA*	*dM/dFe*	Experimental Uncertainty	Regression Misfit
Density (kg/m^3)	2974	42	6	58	15	7
	2928	76		158	15	157
V_p (m/s)	7380	100		-181	47	40
V_s (m/s)	4446	50	-113	-138	24	26
	4379	46		-137	24	44

728

729 Table 5. Linear regression parameters for densities, and compressional and
730 transverse wave velocities of the amphiboles. Derivatives are in units of change per
731 substitutional atom in the formula unit relative to tremolite; the aluminum content
732 varies from 0 to >3, the A-site occupation ranges from 0 to 1, and iron in the C-site
733 can range from 0 to 5. Density and transverse wave velocities have a statistically
734 significant dependence on the A-site occupation. An alternative fit with no
735 dependence on A-site occupation is provided (with a concomitant increase in misfit).
736 The last two columns give experimental and regression misfits.

737

	C_{11}	C_{12}	C_{13}	C_{15}	C_{22}	C_{23}	C_{25}	C_{33}	C_{35}	C_{44}	C_{46}	C_{55}	C_{66}
Diopside Isaak *et al.* 2006	228	79	70	8	181	61	6	245	40	79	6	68	78
Tremolite	107	47	37	-1	186	60	-8	232	-30	79	7	48	50
Hedenbergite Kandelin and Weidner 1988a	222	69	79	12	176	86	13	249	26	55	-10	63	60
Actinolite	93	47	37	-1	167	60	-8	215	-30	67	7	35	36
Jadeite Kandelin and Weidner 1988b	274	94	71	4	253	82	14	282	28	88	13	65	94
Glaucophane Bezacier *et al.* 2010	122	46	37	2	232	75	-5	255	-24	80	9	53	51
$Di_{72}Hd_9Jd_3Cr_3Ts_{12}$ Collins and Brown 1998	238	84	80	9	184	60	10	230	48	77	8	73	82
$Tr_{72}Ac_9Pg_{19}$	122	48	44	-1	185	60	-8	228	-30	74	6	46	48

738

739 Table 6. Comparison of amphibole and clinopyroxene elastic moduli in GPa units.
740 Amphibole moduli are calculated using parameters given in Table 4.

	tremolite	ferro-actinolite	hornblende	tschermakite	pargasite	glaucophane	ferro-glaucophane
Current: Reuss	78(1)	78(1)	88(1)	88(1)	94(1)	88(1)	
H-S	85(1)	85(1)	93(1)	93(1)	99(1)	96(1)	
C91	85				97	96 88(6)	
J10						92(2)	
H03	85	76	94	76	91	96	89

741

742 Table 7. Bulk moduli (GPa units) for selected amphiboles. "Current: Reuss" are
743 isothermal values using the parameters in Table 4 and from Bezacier *et al.* (2010).
744 An adiabatic to isothermal correction was applied to the adiabatic moduli using the
745 thermodynamic properties summarized in Hacker *et al.* (2003a); the correction is
746 ~1.5%. H-S are the average of adiabatic Hashin-Shtrikman bounds. In the current
747 work "hornblende" is a composition based on the Schumacher (2007) average
748 calcium amphibole. The Comodi *et al.* (1991) (C91) and Jenkins *et al.* 2010 (J10)
749 values are based on high pressure isothermal x ray compression measurements.
750 Comodi *et al.* reported values based on linear fits to the data. The second estimate in
751 the C91 row is the re-analysis given by Jenkins *et al.* using a second-order finite-
752 strain equation of state. In the last row (H03) isothermal moduli are taken from
753 Table 1 of Hacker *et al.* (2003a). Uncertainties for the current work are from Table
754 S2. The uncertainties for moduli based on axes compression measurements are
755 reported by Jenkins *et al.* 2010.

	tremolite	ferro-actinolite	hornblende	tschermakite	pargasite	glaucophane	ferro-glaucophane
Current	58	47	57	62	64	64	
H03	49	44	55	44	53	56	52

Table 8. Adiabatic shear moduli (GPa units) for selected amphibole end-members. In the current work "Hornblende" designates a mineral composition based on the Schumacher (2007) average calcium amphibole. The top row lists means of Hashin-Shtrikman bounds based on Table 4 and on Bezacier *et al.* (2010) for glaucophane. Bottom row lists values taken from Table 1 of Hacker *et al.* (2003a).

763

	tremolite	ferro-actinolite	hornblende	pargasite	tschermaktite	glaucophane	ferro glaucophane
Literature V_p km/s	7.1	6.3	7.20	7.3	6.7	7.6	7.0
V_s km/s	4.1	3.6	4.12	4.1	3.8	4.3	4.0
Poisson's ratio	.25	.26	.26	.27	.26	.26	.26
Density gm/cc	2.98	3.43	3.25	3.07	3.04	3.01	3.30
Current V_p km/s	7.4	6.5	7.22	7.7	7.6	7.5	
V_s km/s	4.5	3.8	4.21	4.5	4.5	4.6	
Poisson's ratio	.21	.27	.24	.23	.23	.20	
Density gm/cc	2.97	3.26	3.18	3.11	3.06	3.07	

764

765 Table 9. Isotropic body wave velocities and densities for selected amphiboles.
766 Literature values are from the compilation of Hacker *et al.* (2003a). More significant
767 figures are shown for the hornblende entry since these were based on actual body
768 wave measurements from Christensen (1996). Current values are based on Table 5
769 for calcium amphiboles (using the average calcium amphibole of Schumacher
770 (2007) for hornblende) and Bezacier (2010) for glaucophane.

Table S1. Microprobe chemical analysis of amphiboles. The "reformatted" values are based on PROBE-AMPH (Tindle and Webb, 1994).

Sample number	1	2	3	4	5	6	7	8	9
SiO2	56.22	46.69	43.70	43.78	55.52	45.17	40.51	42.86	41.31
TiO2	0.12	0.96	1.05	1.55	0.02	0.54	1.96	2.95	0.20
Al2O3	1.05	5.87	14.22	11.13	2.41	8.93	7.55	14.96	18.72
FeO	3.28	18.84	11.94	21.95	6.35	15.25	28.43	6.79	6.27
MnO	0.24	1.23	0.10	0.24	0.34	0.39	1.49	0.06	0.11
MgO	21.80	10.25	13.80	7.22	19.65	12.40	2.83	14.51	13.90
CaO	8.30	6.16	9.92	10.28	11.69	10.74	8.79	11.69	12.37
Na2O	4.56	5.74	2.49	2.00	0.54	2.80	3.12	2.50	2.85
K2O	1.48	1.38	0.49	0.50	0.05	1.80	1.64	2.02	0.39
F	2.12	1.46	0	0	0.08	1.56	0.00	0.58	0.01
Cl	0.01	0.06	0	0.03	0.00	0.12	0.00	0.02	0
Cr2O3	0.00	0.02	0.01	0.00	0.32	0.00	0.00	0.02	1.87
Reformatted									
SiO2	56.22	46.69	43.70	43.78	55.52	45.17	40.51	42.86	41.31
TiO2	0.12	0.96	1.05	1.55	0.02	0.54	1.96	2.95	0.20
Al2O3	1.05	5.87	14.22	11.13	2.41	8.93	7.55	14.96	18.72
Cr2O3	0.00	0.02	0.01	0.00	0.32	0.00	0.00	0.02	1.87
Fe2O3	0.92	6.79	11.86	6.49	4.72	3.27	4.58	0.00	1.46
FeO	2.45	12.73	1.27	16.11	2.10	12.31	24.31	6.79	4.95
MnO	0.24	1.23	0.10	0.24	0.34	0.39	1.49	0.06	0.11
MgO	21.80	10.25	13.80	7.22	19.65	12.40	2.83	14.51	13.90
NiO	0.00	0.00	0.00	0.00	0.00	0.00	0.00	0.00	0.00
ZnO	0.00	0.00	0.00	0.00	0.00	0.00	0.00	0.00	0.00
CaO	8.30	6.16	9.92	10.28	11.69	10.74	8.79	11.69	12.37
Na2O	4.56	5.74	2.49	2.00	0.54	2.80	3.12	2.50	2.85
K2O	1.48	1.38	0.49	0.50	0.05	1.80	1.64	2.02	0.39
F	2.12	1.46	0.00	0.00	0.08	1.56	0.00	0.58	0.01
Cl	0.01	0.06	0.00	0.03	0.00	0.12	0.00	0.02	0.00
H2O*	1.14	1.29	2.12	2.01	2.12	1.25	1.85	1.81	2.10
	100.41	100.63	101.03	101.34	99.56	101.28	98.63	100.77	100.24
O=F,Cl	0.89	0.63	0.00	0.01	0.03	0.68	0.00	0.25	0.00
Total	99.51	100.00	101.03	101.33	99.53	100.60	98.63	100.52	100.24

Highlights

- Elastic moduli of nine natural calcium to calcium-sodium amphiboles are reported
- Total aluminum, iron, and A-site occupation accounts for large variance in moduli
- Amphiboles are more elastically anisotropic than previously recognized
- The common preference for Voigt averaging of elastic moduli is challenged
- Seismic responses of rocks with preferred crystal orientations must be re-evaluated

File(s) excluded from PDF

The following file(s) will not be converted:

TableS2_ExperimentalResults.txt

Please click 'Download zip file' to download the most recent files related to this submission.